

Neural Control and Modulation of Swimming Speed in the Larval Zebrafish

Kristen E. Severi,^{1,2,4,6} Ruben Portugues,^{1,5,6,7,*} João C. Marques,³ Donald M. O'Malley,² Michael B. Orger,³ and Florian Engert^{1,7,*}

¹Department of Molecular and Cellular Biology, Harvard University, 16 Divinity Avenue, Cambridge, MA 02138, USA

²Northeastern University Department of Biology, 360 Huntington Avenue, Boston, MA 02115, USA

³Champalimaud Neuroscience Programme, Champalimaud Centre for the Unknown, Doca de Pedrouços, 1400-038 Lisbon, Portugal

⁴Present address: Centre de Recherche de l'Institut du Cerveau et de la Moelle Epinier, Fondation ICM, Campus Hospitalier Pitie Salpetriere, Paris, France

⁵Present address: Max Planck Institute of Neurobiology, Am Klopferspitz 18, Martinsried 82152, Germany

⁶Co-first author

⁷Co-senior author

*Correspondence: rportugues@neuro.mpg.de (R.P.), florian@mcb.harvard.edu (F.E.)

<http://dx.doi.org/10.1016/j.neuron.2014.06.032>

SUMMARY

Vertebrate locomotion at different speeds is driven by descending excitatory connections to central pattern generators in the spinal cord. To investigate how these inputs determine locomotor kinematics, we used whole-field visual motion to drive zebrafish to swim at different speeds. Larvae match the stimulus speed by utilizing more locomotor events, or modifying kinematic parameters such as the duration and speed of swimming bouts, the tail-beat frequency, and the choice of gait. We used laser ablations, electrical stimulation, and activity recordings in descending neurons of the nucleus of the medial longitudinal fasciculus (nMLF) to dissect their contribution to controlling forward movement. We found that the activity of single identified neurons within the nMLF is correlated with locomotor kinematics, and modulates both the duration and oscillation frequency of tail movements. By identifying the contribution of individual supraspinal circuit elements to locomotion kinematics, we build a better understanding of how the brain controls movement.

INTRODUCTION

An important role of the nervous system is the control of locomotion in order to successfully navigate the environment. In the vertebrate brain and spinal cord, this complex task requires the selection of appropriate motor microcircuits to match the demands of any given situation, resulting in smooth and efficient movement. Critical subcortical pathways for the initiation and control of locomotion via the basal ganglia are conserved throughout the vertebrate lineage both anatomically and functionally (Grillner et al., 2013). These regions are linked to form a control pathway in the brain with output in the spinal cord where locomotor central pattern generators (CPGs) reside. One such

motor structure is the mesencephalic locomotor region (MLR), an area where electrical stimulation can initiate locomotion, as first demonstrated in cats nearly 50 years ago, and which functions across locomotor modalities, including walking, flying, and swimming (Cabelguen et al., 2003; Kashin et al., 1974; Shik et al., 1966; Steeves et al., 1987). From this region, signals are conveyed to glutamatergic reticulospinal (RS) cells located in the mid- and hindbrain. These RS neurons are strategically located in the pathway, where visual, postural, and other sensory inputs important for selection of appropriate motor programs are thought to converge (Haehnel et al., 2012; Kohashi and Oda, 2008; Sato et al., 2007). RS neurons excite spinal CPGs (Buchanan and Grillner, 1987; Deliagina et al., 2002; Jordan, 1998) by activating NMDA receptors essential to initiate rhythmic locomotion (Hägglund et al., 2010; McDearmid and Drapeau, 2006; Roberts et al., 2008). This sequence of activation comprises the control or descending pathway for locomotion.

To investigate how neurons in the descending pathway generate commands that produce different speeds of locomotion and how these commands are modulated by relevant sensory inputs, we focused on the RS step in the pathway, which serves as the conduit between the brain and the spinal cord at a critical junction for sensorimotor integration. In the larval zebrafish, the RS population consists of around 300 neurons, many of which are individually identifiable (Kimmel et al., 1982). The activity of this optically accessible population has been linked with locomotion in response to a variety of sensory stimuli (Huang et al., 2013; Kimura et al., 2013; Koyama et al., 2011).

One of these innate sensory-driven locomotor behaviors is the optomotor response (OMR) (Bilotta, 2000; Neuhauss et al., 1999), in which larvae respond to whole-field visual motion (Maaswinkel and Li, 2003; Orger et al., 2000) by swimming and turning to maintain a stable position with respect to their visual environment (Portugues and Engert, 2009). In a survey of RS activity in response to visual stimuli driving the OMR (Orger et al., 2008), the most prominent group activated by visual stimulation that specifically elicits forward-directed locomotion was found in the nucleus of the medial longitudinal fasciculus (nMLF), a cluster of RS cells in the midbrain which extends dendrites toward retino-recipient areas, and projects its axons to the spinal cord

(Gahtan et al., 2005; Kimmel et al., 1982; Wang and McLean, 2014 [this issue of *Neuron*]). This structure is known to be multimodal and is active in response to a variety of stimuli as well as during spontaneous swimming, and is further believed to be implicated in a broad range of intensities of locomotion (Sankrithi and O'Malley, 2010).

In this study we aim to characterize the different kinematic parameters that are dynamically modulated during swimming at different speeds. Larvae swim in units called "bouts," where each individual bout is characterized by a discrete number of tail oscillations that propel the larva through the water. We show that different speeds of locomotion are accomplished not only by changing the speed of these oscillations, but also through a dynamic interplay between the locomotor gait, and the duration, intensity, and rate of movement episodes. A quantitative description of the behavior gives us a starting point to step backward through the circuit and ask how the upstream activity in the RS cells, specifically the nMLF, relates to these kinematic parameters and contributes to this modulation. We observe correlations between activity in identified nMLF neurons and both the visual stimulus and the specific behavioral elements we identify as signatures of changing locomotor speed. We use stimulation and ablation of these cells to assess their necessity and sufficiency in modulating the various behavioral parameters. With *in vivo* two-photon calcium imaging in an awake, behaving, minimally invasive preparation, we present evidence for selective locomotor modulation by identified neurons. This study allows us to dissect the nature of activity in descending inputs that are important in controlling the speed of locomotion in an intact behaving animal.

RESULTS

Modulation of Locomotor Activity in Response to Whole-Field Visual Motion

In response to optomotor gratings moving at speeds from 0 to 40 mm/s, larval zebrafish adjust their locomotor speed to maintain their position relative to the moving grating. Relevant kinematic parameters were measured in an effort to quantitatively describe this behavioral response. Freely swimming 6-day-post-fertilization (dpf) wild-type (WT) larvae were individually presented with sinusoidal striped patterns moving at different speeds from below, while high-speed video was acquired (Figure 1A). Analysis of the raw video (Figure 1B; [Experimental Procedures](#)) allowed us to calculate relevant kinematic variables (Figures 1C–1I). We first confirmed that larvae increase their average swim speed as grating speed increases (Figures 1C and 1D). Over the course of a trial lasting several seconds (Figure 1C), they were able to match grating speeds up to 20 mm/s, but their speed plateaus for gratings moving at faster velocities (Figure 1D).

Larvae swim intermittently in what has been described as a beat-and-glide mode. This includes a bout period when active swimming is performed and the tail is oscillating, followed by an interbout period of varying duration when the larva is not actively swimming, but is either coasting or stationary. A close look at the instantaneous swimming speed (Figure 1C) revealed the cyclic nature of the intermittent swimming style in the peaks and troughs of each line.

We next analyzed individual bouts and interbouts and their contribution to average swimming speed. We observed an increase in average distance per bout with grating speed (Figure 1E). Some of this could be accounted for by the lengthening of bout duration as grating speed increased within the range 0–10 mm/s (Figure 1F), whereas the increase beyond 10 mm/s is accompanied by a rise in the average tail-beat frequency (TBF), which was only modulated for bouts elicited by a grating moving faster than 10 mm/s (Figure 1G). A faster grating led larvae not only to modulate their swim bouts, but also to elicit them more often: an interbout duration of 1 s for a stationary grating became 200 ms by the time the grating moved faster than 10 mm/s (Figure 1H). The latency of the motor response from the initiation of the grating motion was also modulated by grating speed (Figure 1I). We saw a significant decline in latency as the speed of the grating increased, indicating that a faster grating elicited a locomotor response more quickly.

From these data we can identify relevant kinematic variables that are dynamically changing in freely swimming larvae over the range of grating speeds tested. Changes in bout duration, interbout duration, and latency appear to contribute at slower speeds, while changes in TBF are the major contributor at faster speeds. Despite this variety of factors that determine swimming speed, the larva is able to maintain a tight correlation of its own swimming speed with that of moving gratings up to 20 mm/s.

Larval Swim Bouts Cluster into Fast and Slow Types

Having determined that larvae swim faster when presented with faster OMR stimuli, we wanted to know whether they do so by continuously modulating a single type of bout or whether, as for many vertebrates, they are able to engage distinct gaits to locomote at different speeds. In the first scenario, we expect bouts to be distributed continuously throughout parameter space. Alternatively, if locomotor output is organized discretely and different types of bout are recruited, we expect the kinematic parameters across the entire bout population to cluster into two or more distinct groups.

For slow stimuli trials, the bouts formed a single cluster in a space defined by head yaw, mean TBF, rostral bend amplitude, and maximum TBF (Figures 2A and [S1 available online](#)). As the grating speed increased, the original cluster shifts progressively in this space, indicating a modulation of the slow swim bout. In addition, a second cluster emerged such that for fast-moving grating trials, two distinct distributions with minimal overlap were observed (Figure 2B). Based on these clusters, we categorized each bout as either a slow bout or a fast bout ([Experimental Procedures](#)). We plotted the density of bouts in parameter space defined by selected kinematic variables as quantified in our assay (Figures 2C and [S2](#)). To assess the consistency of the categorization, we used four different kinematic parameters and found agreement in all cases (Figure 2D). The fraction of fast bouts elicited by a drifting grating changes continuously from ~4% for slow-moving stimuli to ~50% for stimuli moving at 20 mm/s or faster.

To test whether the kinematic parameters of these two different types of bouts vary with stimulus speed, we repeated the analysis of Figure 1 for slow and fast bouts, respectively ([Movie S1](#)). Both bout types showed a progressive modulation of speed and distance (Figures 2E–2G) in response to different

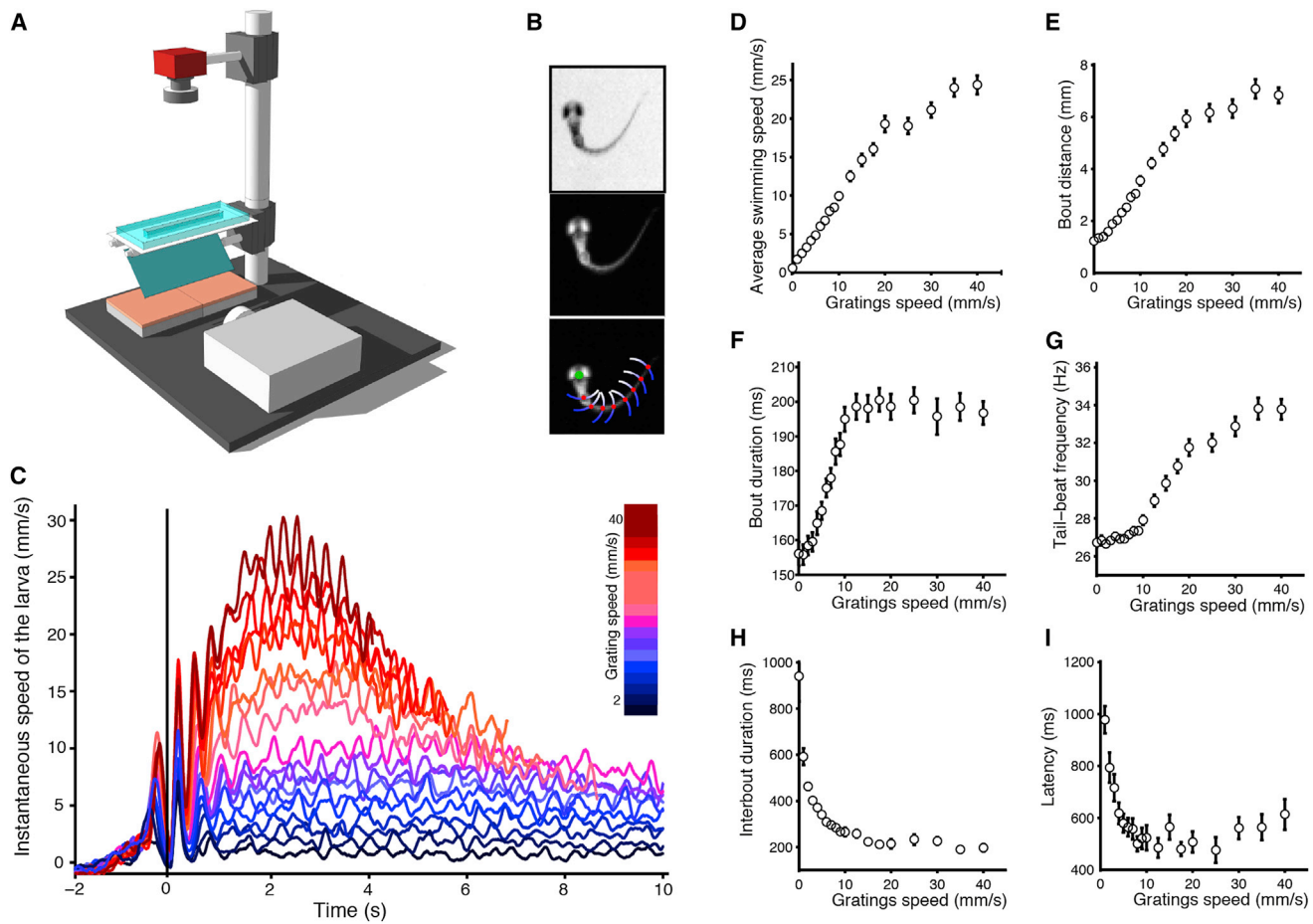


Figure 1. Larval Swimming Speed Depends on OMR Grating Speed

Relevant kinematic variables, which describe larval zebrafish swimming, are plotted against grating speed over a range of 0–40 mm/s.

(A) Schematic of experimental rig for freely swimming larvae. High-speed video was acquired from above with drifting gratings projected on a screen below the arena, and larvae illuminated with IR light.

(B) Image processing involved background subtraction, determination of the global maxima (green point), and tail curvature (Experimental Procedures; Supplemental Information). Scale bar, 2 mm.

(C) Instantaneous swimming speed versus grating speed. Traces are aligned such that 0 on the x axis is the initiation of the first bout in the direction of the stimulus motion. For data to the right of the black line (left of this line indicates orienting maneuvers the larva uses to align its body with the axis of motion of the grating), we see the difference in swimming speed as a function of grating speed, and also the timing during which this swimming speed varies with respect to initiation of grating motion. (D)–(I) represent data from 52,938 bouts from 45 freely swimming larvae.

(D) Average swimming speed during trial (mm/s) versus grating speed.

(E) Average bout distance (mm) versus grating speed.

(F) Average bout duration (ms) versus grating speed.

(G) Average tail-beat frequency (TBF) elicited during a bout (Hz) versus grating speed.

(H) Average interbout duration (ms) versus grating speed.

(I) Latency (ms) versus grating speed. Error bars indicate SEM.

grating speeds, although slow bouts plateaued at just under 20 mm/s bout speed and 4 mm bout distance. Note that the fraction of fast bouts elicited was smaller than 10% for grating speeds under 10 mm/s (Figure 2D). Mean and maximum TBF (Figures 2H and 2I) were relatively constant for slow bouts, but were strongly modulated with grating speed for fast bouts, while the opposite was true of bout duration (Figure 2F). In summary, during slow bouts larvae performed different numbers of oscillatory cycles at the same TBF resulting in longer bouts, whereas for fast bouts larvae swam with different TBFs over a fixed duration.

These results allowed us to quantitatively analyze the locomotor response of larvae when presented with moving gratings at various speeds. In response to slow grating speeds, larvae performed slow bouts. As the grating speed increased from 0 to 10 mm/s, the duration of these bouts increased as did their speed, resulting in bouts that spanned a greater distance, and the interbout interval was reduced. When grating speeds reached 10 mm/s, the rate and performance of slow bouts saturated, and larvae began recruiting fast bouts. As the stimulus speed increased from 10 to 40 mm/s, these fast bouts were

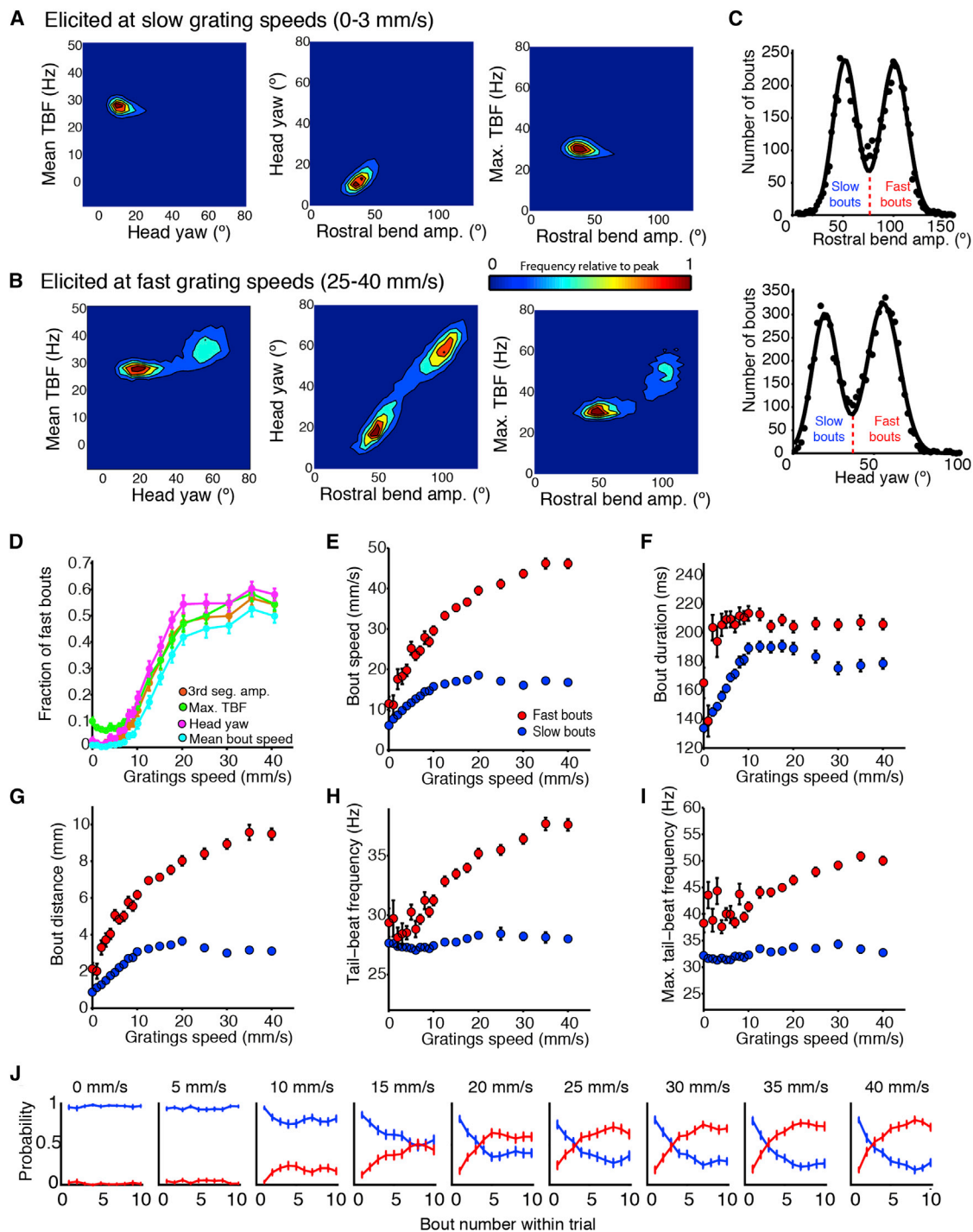


Figure 2. Larvae Swim by Eliciting Bouts that Cluster into Two Types

(A) Bouts elicited at slow grating speeds. Joint distributions of several pairs of relevant kinematic parameters including mean and maximum TBF, head yaw, and rostral bend amplitude.

(B) Distributions of the same parameters as in (A) for bouts elicited at fast grating speeds. Slow pool data (0, 1, 2, and 3 mm/s gratings) and fast pool data (25, 30, 35, and 40 mm/s gratings; see Figure S1).

(C) Fitting of rostral bend amplitude (upper) and head yaw (lower) parameters with binormal distributions to establish the threshold between fast and slow bouts plotted below (Figure S2).

(D) Fraction of bouts that are fast as determined by different kinematic parameters: yaw, rostral bend amplitude, mean bout speed, and maximum TBF.

(E) Average bout speed (mm/s) versus grating speed for fast (red) and slow (blue) bouts.

(legend continued on next page)

recruited more frequently. Their TBF and speed increased with grating speed resulting in more vigorous bouts.

When presented with a whole-field moving visual stimulus, do larvae estimate their speed and then recruit the appropriate locomotor output, or do they start with a slow bout and then recruit faster bouts if the outcome of the previous motor output was insufficient? We computed the probability of a bout being slow or fast according to its position in the sequence of bouts for a trial with a given stimulus speed (Figure 2J). In fast trials, larvae often began with slow bouts and only later recruited fast bouts. This phenomenon was consistent with behavioral responses in a restrained motor-learning assay, where larvae adjusted their motor output if it did not match their expectation (Ahrens et al., 2012; Portugues and Engert, 2011).

Restrained Larvae Performing the OMR Only Use Slow Bouts

With a view to monitoring neural activity in a restrained or paralyzed larva, we characterized the changes in kinematic variables in head-restrained larvae in an arrangement where the head remained stationary in agarose, but the tail was free to move, and larvae were still able to reliably perform the OMR by moving their tails in response to drifting gratings. Larvae viewing drifting gratings in this open-loop setup increased the duration of bouts (Figure 3A) and decreased both the interbout duration (Figure 3B) and the latency to initiate swimming (Figure 3C) with increasing grating speed, consistent with the behavior of freely swimming larvae. These parameters, along with TBF, were the focus of our analysis since other parameters investigated in Figures 1 and 2 do not apply to head-restrained larvae.

In order to identify what types of bouts larvae were performing in the head-restrained preparation, we compared the distribution of the maximum TBF of bouts to that obtained in the freely swimming experiments reported in Figures 1 and 2, where larvae perform both slow and fast bouts. We used maximum TBF as a kinematic parameter because we expected it to be least disrupted by the restrained preparation. For restrained larvae (Figure 3D), bouts most often contained a maximum TBF around 30 Hz, even at fast grating speeds. The shape of these distributions matches that observed in freely swimming larvae (Figure 3D) for slow speeds, but differs significantly at fast grating speeds. At fast speeds, freely swimming larvae executed bouts that contain maximum TBFs often exceeding 65 Hz, which was rarely observed in restrained larvae. These frequencies are those associated with fast bouts, from which we conclude that in the restrained preparation larvae robustly perform the OMR to gratings moving at different speeds, but do so mainly by modulation of slow bouts. Therefore, we focus on the modulation of the speed of slow bouts, which we consider to be kinematically similar to the “slow swim” gait described previously (Budick and O'Malley, 2000). These behavioral experiments provided

an essential starting point from which to investigate the neural control of this motor behavior. The delicate adjustment of kinematic variables resulted in the larva responding to a faster grating with motor output enabling it to cover a greater distance over time.

Laser Ablation of nMLF Cells Reduces Maximum Swimming Speed in Response to Drifting Gratings

Next, we asked whether removal of descending neurons would affect swimming speeds, thus implicating them in speed modulation. Following previously described methods (Huang et al., 2013; Orger et al., 2008), we used two-photon laser ablation of bilaterally symmetrical individual neurons to test the effect on optomotor swimming in response to various speeds of visual gratings (Experimental Procedures). The nMLF is a nucleus located in the midbrain consisting of ~20 neurons on each side (Figure 4A; Movie S2). In light of previous work describing activity of different RS cell populations in response to presentations of moving gratings (Orger et al., 2008), we hypothesized that the nMLF was a strong candidate for controlling forward optomotor swimming, since it showed bilaterally symmetric responses, whose direction tuning matched the behavioral tuning of forward swims. We targeted three groups within the RS neurons for laser ablation: large cells of the nMLF, cells in the RoM cluster, and the Mauthner cells (Figure 4A). Eight of the nMLF neurons are larger in size than the others, MeLr, MeLc, MeLm, and MeM, with one of each type in each half of the brain (Kimmel et al., 1982). We always ablated at least four of these eight neurons, a small subset of the nMLF by number, but the only individually identifiable cells across larvae. We suspected that ablating fewer would result in imperceptible phenotypes. In control regions, four to eight RoM neurons were ablated, or alternatively both Mauthner cells. We recorded the behavioral response to several grating speeds before and after laser ablation of targeted cells (Figure 4B). The behavior in RoM-ablated larvae and Mauthner cell-ablated larvae was similar and is pooled below. Compared with preablation larvae, only the nMLF-ablated larvae showed a consistent and significant deficit in achieving high speeds of swimming in response to visual stimuli (Figures 4C, 4D, and S3). This finding applied to all of the parameters we recorded, including bout duration, maximum TBF, bout distance, and bout speed, indicating a general deficit in modulation of swimming speed in response to a large range of grating speeds as compared to controls which showed no deficit.

Strength of Stimulation of the nMLF Is Correlated with Aspects of Elicited Swimming

We asked if activation of the nMLF produced a locomotor response by developing a protocol for direct electrical microstimulation of the nMLF to establish the sufficiency of nMLF activity in eliciting swimming. When electrical pulses of a given intensity

(F) Average bout duration (ms) versus grating speed.

(G) Average bout distance (mm) versus grating speed.

(H) Average TBF (Hz) versus grating speed.

(I) Average maximum TBF elicited during a bout (Hz) versus grating speed.

(J) Probability that a bout will be slow or fast for different grating speeds plotted by the order of bouts elicited (bout number) independent of time. Error bars indicate SEM (n = 52,938 bouts from 45 larvae).

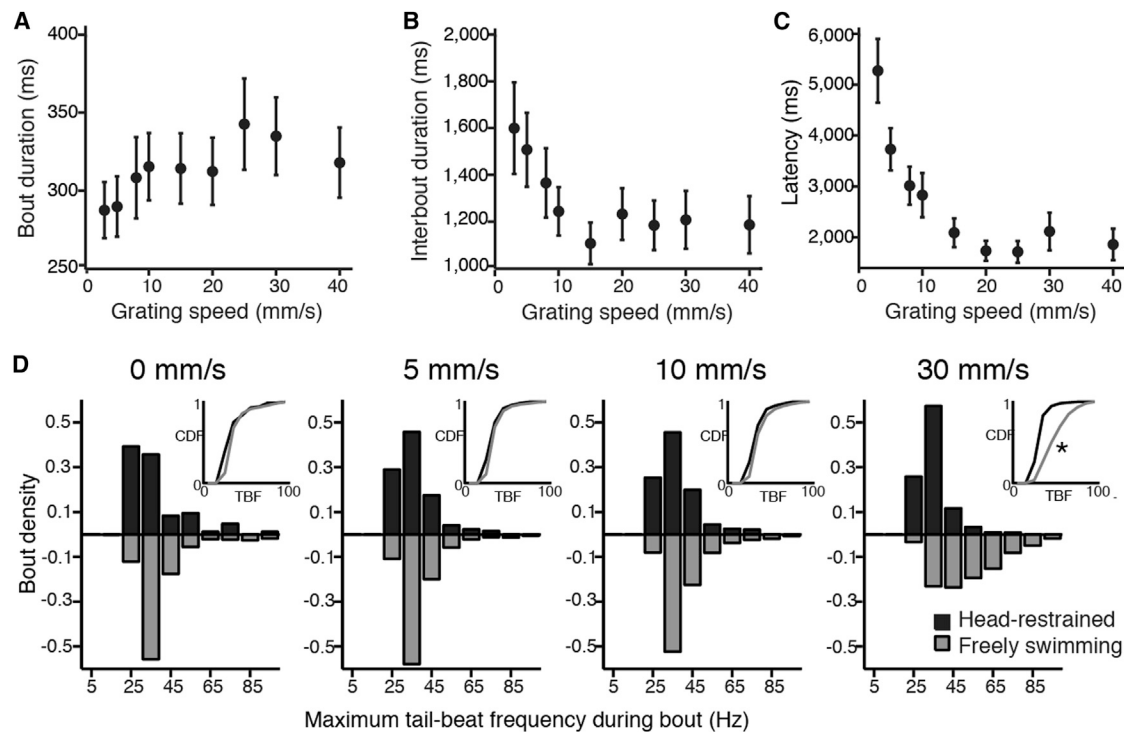


Figure 3. Restrained OMR Kinematic Parameters

By restraining the head in agarose, but leaving the tail free to move, we extracted kinematic parameters from restrained swimming to compare with free swimming ($n = 25$ larvae).

(A) Mean bout duration (ms) versus grating speed.

(B) Interbout duration (ms) versus grating speed.

(C) Latency (ms) versus grating speed.

(D) Histograms of the number of bouts elicited by maximum TBFs for four grating speeds: 0, 5, 10, and 30 mm/s in head-restrained (black) and freely swimming (gray) larvae (speed 0 mm/s, 84 restrained [res] bouts and 2,427 free-swimming [fs] bouts; speed 5 mm/s, 2,748 res bouts and 5,092 fs bouts; speed 10 mm/s, 2,698 res bouts and 3,334 fs bouts; speed 30 mm/s, 1,472 res bouts and 1,631 fs bouts). The inserts show the cumulative distribution function for both the histograms for comparison. Only the last set of histograms (elicited with a 30 mm/s grating) were significantly different from each other (Kolmogorov-Smirnov [KS] test, $p < 0.01$).

and frequency were delivered to the nMLF ([Experimental Procedures](#)), larvae responded with distinct locomotor patterns ([Figure 5A](#)). The cyclic nature, TBF, and maximum bend position along the tail indicate these movements were not struggle or escape responses. Calcium imaging using calcium green dextran ([Figure 5B](#)) verified that nMLF cells were activated during this induced locomotion. These data were collected from non-paralyzed larvae, so imaging trials could be interleaved with high-speed behavioral movies in the same larva. We observed consistent activation concurrent with the start of each pulse train, and calcium indicator fluorescence rose over the course of the train delivery.

We modified the stimulation parameters by increasing both the current and the frequency of the pulses delivered. Increasing the current had no significant effect (data not shown), but increasing the pulse frequency resulted in an increase in bout duration ([Figure 5C](#)) and an increase in maximum TBF ([Figure 5D](#)). This suggests that the stimulated neurons were activated more strongly under these higher-frequency conditions. We confirmed this by measuring the maximum $\Delta f/f$ of the calcium response to the varying stimulation parameters, and

concluded that the frequency of stimulation modified the amplitude of the calcium signal in large nMLF neurons ([Figure 5E](#)). It is worth noting that the kinematic values for the data in [Figure 5](#) have a similar range to the data in freely swimming and restrained larvae swimming in response to drifting gratings ([Figures 1 and 3](#)).

To confirm these effects were dependent on stimulation of a specific region containing the nMLF, we used the minimum threshold for activation and moved the stimulation pipette incrementally away from its initial position adjacent to the nMLF somas, while testing behavioral and nMLF responses at each position ([Figure S4](#)). We observed a response in $<5\%$ of trials at distances greater than 60 μm . In all larvae ($n = 10$), we observed that a failure to elicit a behavioral response always correlated with a failure to elicit a calcium response, and we always saw either bilateral activation of the entire nucleus across both sides of the midline or no activity at all. These data indicated that electrical stimulation of the nMLF was sufficient to evoke swimming, and that the stimulation parameters which modified bout duration and TBF also modified activity in the nMLF.

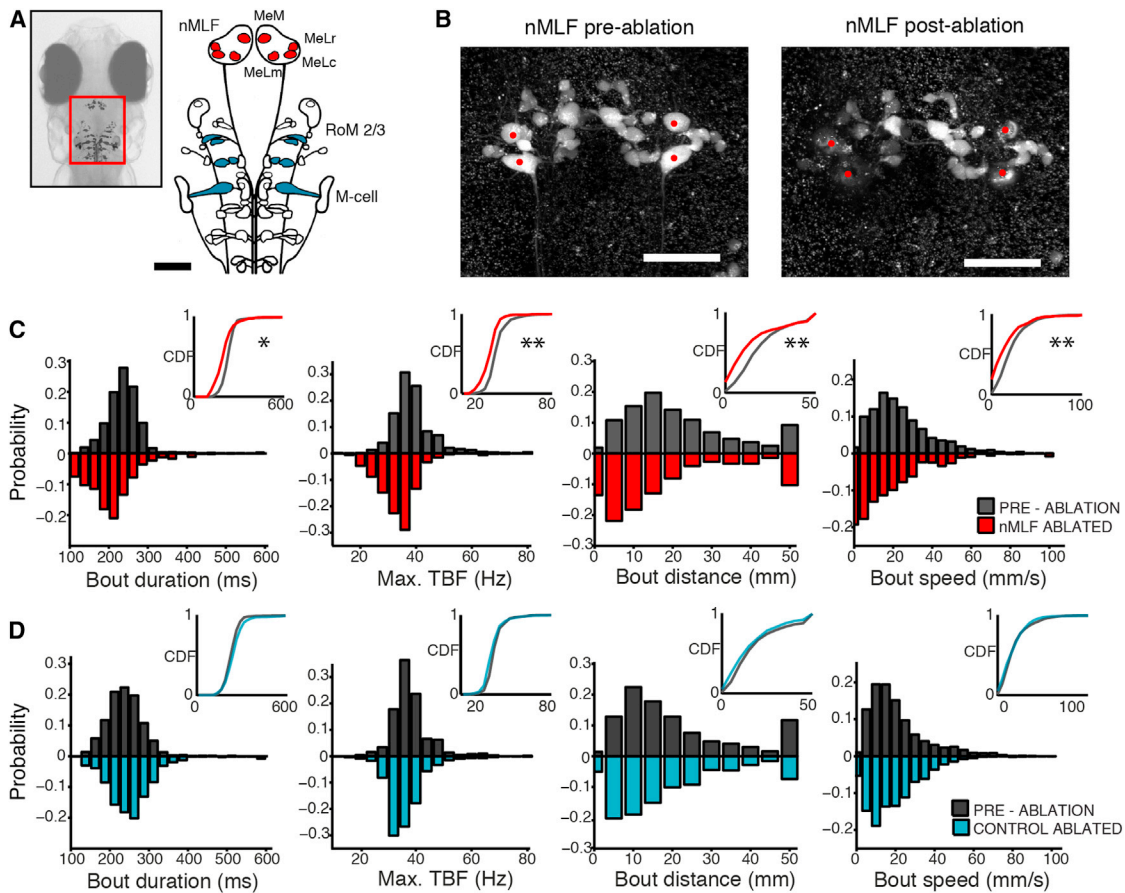


Figure 4. Laser Ablation of the nMLF Reduces OMR-Induced Swimming Speed

(A) Inset: head of a larval zebrafish. Image of RS labeling is overlaid in approximate location. Schematic of RS neurons in the mid- and hindbrain labeled by spinal backfill with large nMLF neurons (red) and control ablation neurons (blue) (either a subset of RoM neurons from the second and third rhombomeres or the Mauthner cells). Scale bar, 50 μ m.

(B) Maximum-intensity z-projection of image stacks taken of the nMLF before and 4 hr postablation. Targeted cells are indicated by red dot. Scale bar, 25 μ m.

(C) Histogram of the probabilities of various kinematic parameters of swimming occurring before (gray, 17 larvae, 1,506 bouts) and after (red, same larvae, 806 bouts) ablation of the nMLF. From left to right: the bout duration (ms), the maximum TBF (Hz), the bout distance (mm), and the bout speed (mm/s). The cumulative distribution functions pre- and postablation are plotted in the upper right. The distributions of the two histograms are significantly different in all cases (KS test, * $p < 0.05$, ** $p < 0.01$).

(D) Histogram of swimming speed before (gray, 10 larvae, 1,364 bouts) and after (blue, same larvae, 1,012 bouts) ablation of control neurons for the same kinematic parameters. The cumulative distribution functions pre- and postablation are plotted in the upper right and are not significantly different in any case.

Population Activity in the nMLF as Grating Speed Varies

We investigated the activity of the population of nMLF neurons during presentations of gratings of different speeds. Is there a greater number of nMLF neurons recruited as grating speed increases, or do activity patterns of nMLF neurons vary with grating speed? To address these questions, we used *in vivo* two-photon calcium imaging of nMLF neurons loaded with calcium green dextran in paralyzed larvae presented with drifting gratings moving at one of five speeds (Figure 6A). We were able to monitor the population as a whole using this labeling technique, including the eight individually identifiable large cells (MeLr, MeLc, MeLm, and MeM) and small cells in the left and right clusters (Figure 6B). An example of calcium responses of three cells to these different stimuli is shown in Figure 6C. These calcium responses were consistent with targeted cell-attached

electrophysiological recordings from large nMLF neurons (Figure S5). We observed no lateralized differences in responses, so examples from the left and right sides of the midline were pooled. The maximum $\Delta f/f$ of the calcium response changed across speeds (Figure 6D) and did so differently for the large and small cells: small cell responses appeared to be similar across speeds and their latency was found to decrease slightly less as grating speed increased (Figure 6E). We observed a marked difference between the MeM cells and the other three types of large nMLF cells, the MeL cells. MeM cells showed a significant decrease in activity for the fastest-moving grating speed, and the latency to peak signal was 2 s longer across all speeds.

Monitoring neural activity using calcium imaging allowed us to investigate whether recruitment of neurons to the active pool

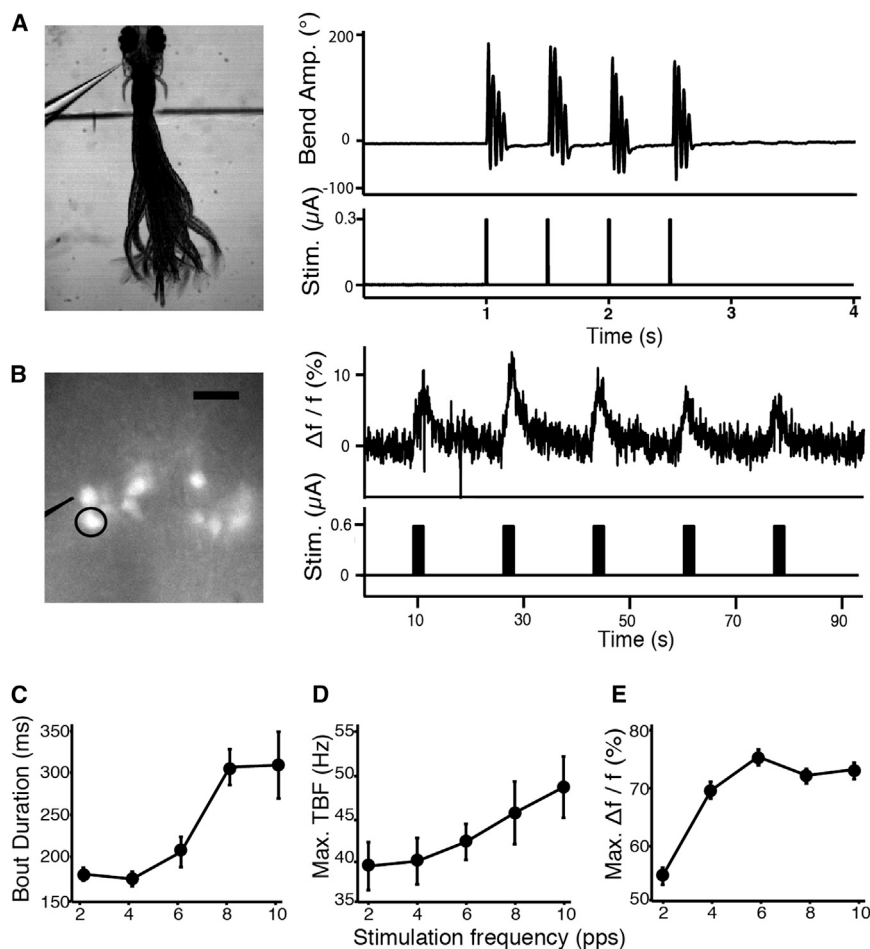


Figure 5. Electrical Stimulation of the nMLF Elicits Swim-like Behavior and Neural Responses Modulated by the Stimulation Intensity

(A) Behavioral responses during midbrain electrical stimulation. Left, image of a larva responding to midbrain electrical stimulation. Electrode position can be seen as well as border of agarose removed to free the tail. Right, recorded locomotor responses elicited by nMLF stimulation.

(B) Calcium activity in the nMLF during electrical stimulation. Left, reference image of nMLF neurons, labeled with Texas red dextran, viewed with both bright-field and epifluorescence illumination. Stimulation pipette is outlined and the left MeLc neuron (calcium response shown in E) circled. Right, raw calcium trace from nMLF left MeLc cell during midbrain electrical stimulation and accompanying stimulus of five trains.

(C) Average bout durations from swim-like behavioral responses to midbrain electrical stimulation ($0.45 \mu\text{A}$) over five different stimulation frequencies (2, 4, 6, 8, and 10 pulses per second). $n = 13$ larvae and 4,373 bouts. Error bars indicate SEM. A three-way ANOVA was used to determine statistical significance; frequency of stimulation was significant ($p < 0.0001$). Across larvae, behavior was always significantly different from each other ($p < 0.0001$).

(D) The average maximum TBFs calculated per bout and averaged across larvae during bouts elicited by electrical stimulation ($n = 13$ larvae and 4,373 bouts). Frequency of stimulation significantly modulated maximum TBF ($p < 0.0003$). Stimulation parameters and statistical methods identical to those in (C).

(E) Calcium responses to midbrain electrical stimulation from identifiable nMLF cells for three different currents over five different stimulation frequencies. Maximum $\Delta f/f$ response for the average of all cells across all larvae ($n = 16$ larvae, 101 cells). Error bars indicate SEM.

was growing as grating speed increased. We plotted the fraction of cells that were active when presented with the various speeds of moving grating (Figure 6F) and found large cells were active 100% of the time. However, only a fraction of small cells responded, but this fraction remained constant at around 80% across grating speeds. We concluded from these results that no recruitment of nMLF cells was occurring as the grating speed increased. This suggested that if the nMLF was involved in behavioral modifications with increasing speed, as was indicated by the previous results, this occurred as a result of the change in activity of already active cells rather than the recruitment of previously inactive cells. We found the largest modulation of activity in the large cells, which we focused on in following experiments.

Correlation of nMLF Calcium Activity with Locomotion in Restrained, Actively Swimming Larvae

To clarify the role of individual nMLF neurons in modulating the various swimming parameters, we monitored their activity using two-photon calcium imaging in the head-restrained preparation (Figure 7A; Movie S3) to correlate neuronal activity with both sen-

sory input (grating motion) and restrained active swimming with minimal motion artifacts (Experimental Procedures; Figure S6). It should be noted that calcium signals persist when the larva is paralyzed, and motor output is recorded by ventral roots (Figure S7). A portion of a representative experiment is shown in Figure 7B, which involved alternating 10 s periods of a static grating with forward-grating motion at different speeds (5, 10, and 30 mm/s). In these experiments, larvae performed the majority of swim events while presented with the two slower-moving gratings (Figure 7C). We imaged the nMLF, which had previously been labeled with calcium green dextran, and presented the visual stimuli in each imaging plane (Experimental Procedures; Supplemental Information). The fluorescence traces of six cells recorded simultaneously are shown in blue. We also monitored tail motion, shown in black (higher temporal resolution shown in Figure 7D). In this way we could correlate the activity of individually identified neurons with specific behavioral parameters from individual bout events recorded simultaneously.

We first asked whether the activity of the large nMLF cells correlated best with sensory input or with motor output (Figure 7E). To calculate the sensory-triggered activity, we averaged

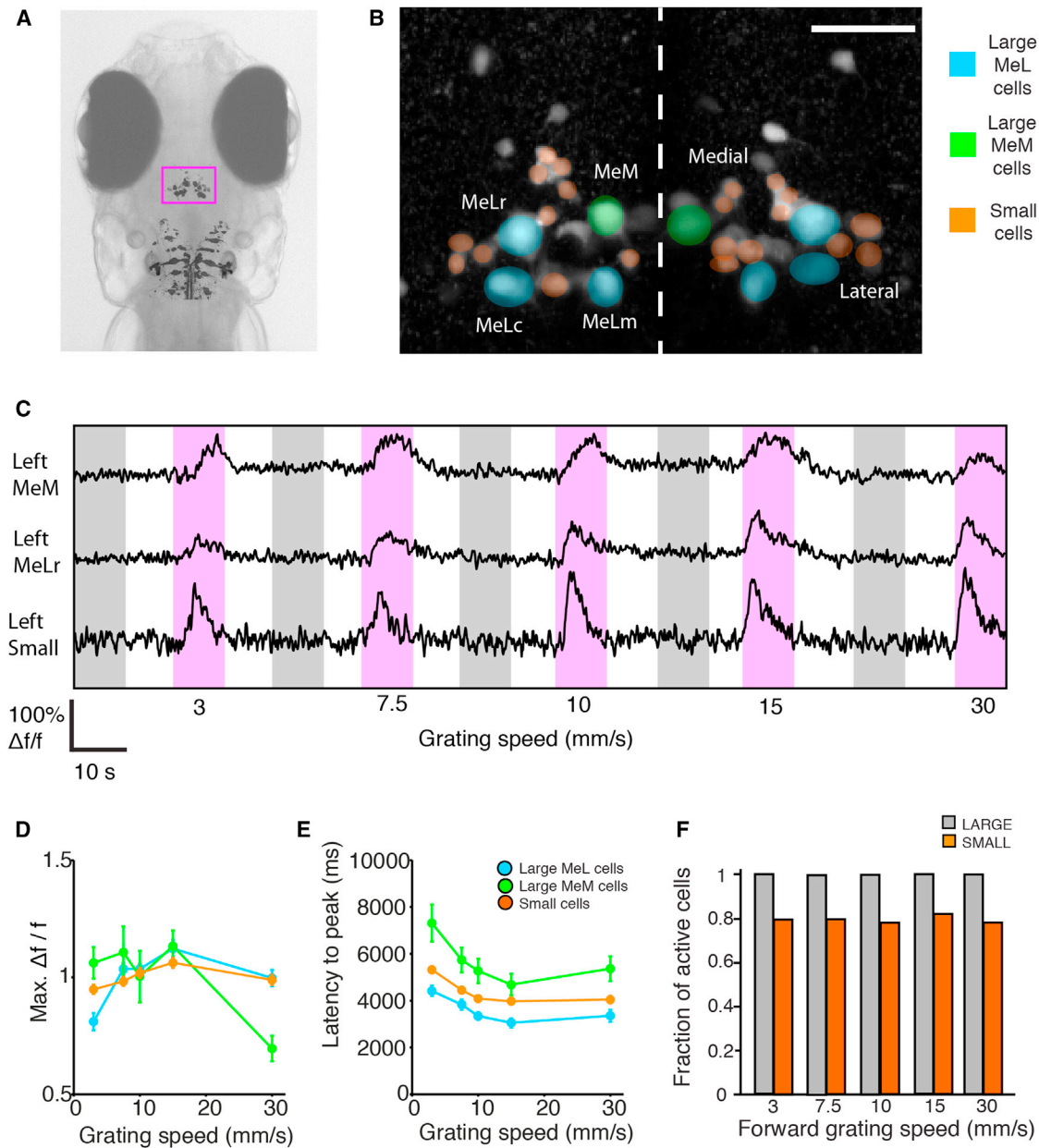


Figure 6. Monitoring Activity of the nMLF Population with Two-Photon Calcium Imaging

(A) Head of a larval zebrafish. The nMLF is located in the magenta rectangle $\sim 140\text{--}200\ \mu\text{m}$ from the dorsal surface. Image of RS labeling including nMLF neurons is overlaid in approximate location.

(B) Z-projection of nMLF neurons. Cells are labeled via spinal injections of calcium green dextran. Cells color coded as small (orange), large MeL cells (blue), or large MeM cells (green).

(C) Calcium signals recorded in several cells simultaneously. Periods of stimulus presentation are indicated by magenta and gray shaded areas for forward and backward grating motion, respectively. Grating speed in mm/s is indicated below.

(D and E) The maximum $\Delta f/f$ calcium response and the latency to the peak of the calcium signal, respectively, during stimulus presentation as a function of grating speed for the large and small cells. Responses were recorded from individual cells, and when no significant differences were observed between groups, responses were pooled for clarity. Error bars indicate SEM. Large cells; MeLr ($n = 25$), MeLc ($n = 23$), MeLm ($n = 6$), MeM ($n = 10$), all ($n = 64$). Small cells; left lateral ($n = 59$), left medial ($n = 43$), right lateral ($n = 57$), right medial ($n = 31$), all ($n = 190$). $n = 21$ larvae.

(F) The fraction of active cells during forward-moving gratings across grating speeds. Cells were classified as active if their $\Delta f/f$ was above a 10% threshold.

the fluorescence for each of the large nMLF cells over all stimulus presentations and separated these into presentations during which the larva executed bouts and those that did not elicit

swimming (Figure 7E). We found that nMLF cells were only active in presentations during which bouts occurred. When shown a forward-moving grating, larvae typically performed a

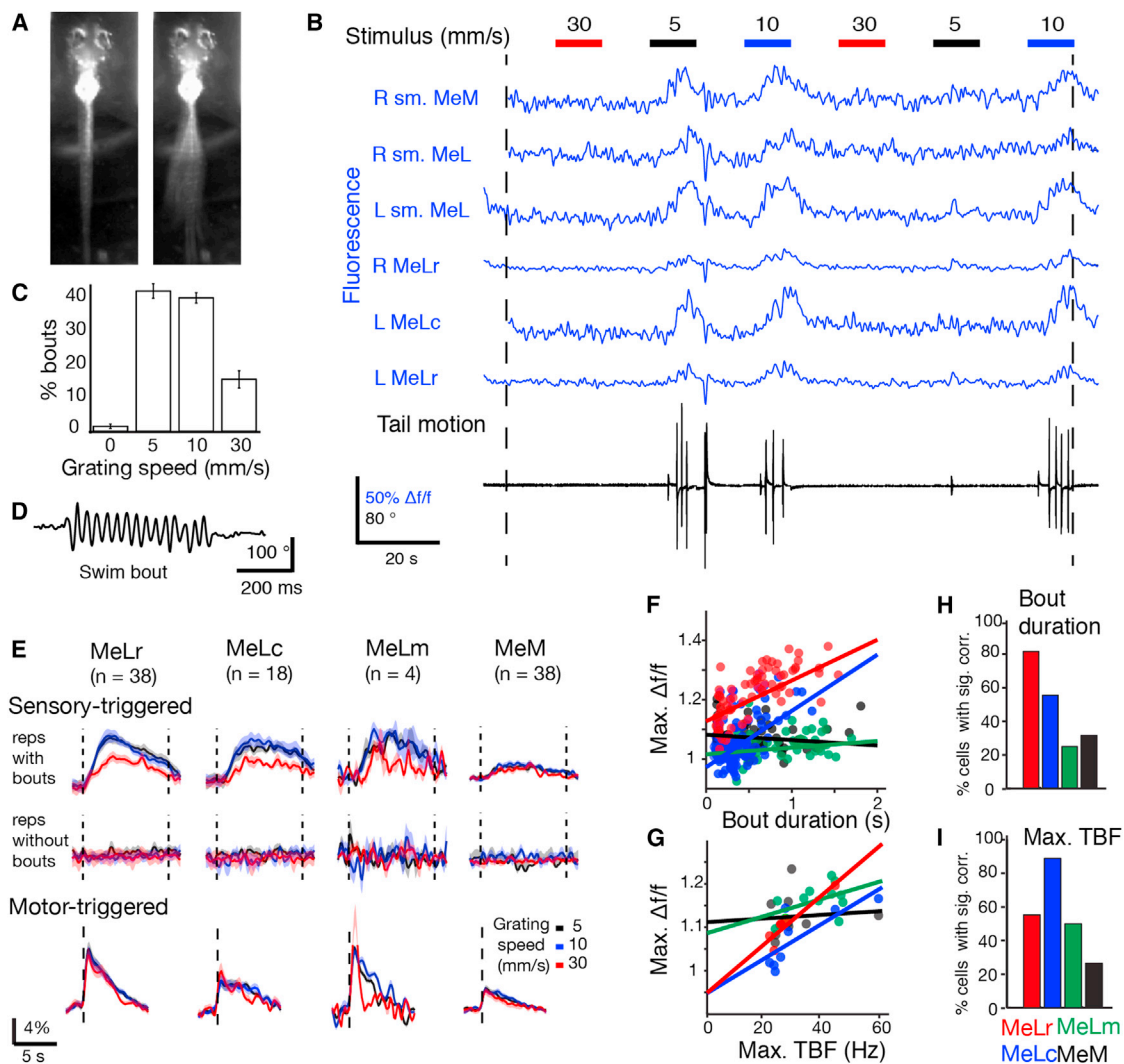


Figure 7. Calcium Imaging of nMLF Activity in Behaving Larvae

(A) Image of a larval zebrafish in the two-photon imaging setup while motionless (left) and a projection while performing a slow swim (right).

(B) Sample of data acquired during an experiment. Data shown correspond to imaging one plane of the nMLF for two minutes. In each plane, six 10 s periods of a static grating were interleaved with six 10 s periods of a forward-moving grating at 5, 10, or 30 mm/s (shown at top). Grating speeds were repeated twice per plane. In each plane several nMLF cells were visible, and their fluorescence traces could be determined (shown in blue). The setup allows simultaneous monitoring of tail movement during calcium imaging (cumulative tail angle shown in black, see D for better resolution).

(C) Percentage of bouts elicited by the different grating speeds presented.

(D) Tail motion trace for a representative swim bout recorded in the setup.

(E) Sensory-triggered calcium responses (top and middle) for each of the large nMLF cell types grouped into repetitions during which larvae performed swim bouts (top) and those during which larvae did not (middle) and color coded for the speed of the grating that was presented (black, blue, and red for 5, 10, and 30 mm/s, respectively). Motor-triggered responses for the four large cell types are shown in the bottom, color coded similarly. Data shown are the average of all the cells labeled from 20 larvae.

(F) Scatter plot for all swim bouts recorded in a sample larva of bout duration versus the maximum calcium response for each of the large nMLF cell types (MeLr, MeLc, MeLm, and MeM in red, blue, green, and black, respectively) together with the best fit arising from linear regression.

(G) Scatter plot for all swim bouts recorded in a sample larva of maximum TBF versus the maximum calcium response for each of the four large nMLF cell types together with the best fit arising from linear regression.

(H) Percentage of cells for the four large nMLF cell types that were found to have a significant correlation with bout duration (31/38, 10/18, 2/4, and 12/38 from 20 larvae).

(I) Percentage of cells for the four large nMLF cell types that were found to have a significant correlation with the maximum TBF (21/38, 16/18, 2/4, and 10/38 from 20 larvae).

forward-swim bout such as in [Figure 7D](#). Rarely, larvae performed other behavioral maneuvers ([Figure S6C](#)).

We subsequently aligned the calcium activity of each cell based on the timing of bout events to find the motor-triggered response of the large nMLF cell types ([Figure 7E](#), bottom row). The motor-triggered responses were similar across speeds. We concluded that activity in the nMLF was motor related, and that the larger sensory-triggered activity at 5 and 10 mm/s grating speed is solely a result of the fact that these speeds elicit more bouts ([Figure 7C](#)). We observed that the responses measured in MeMs were generally smaller than those measured in the MeLs. The results in [Figure 7E](#) suggest nMLF activity in response to optomotor gratings is not sensory related, but is rather locked to the timing of swim bouts.

We analyzed the correlation of nMLF activity with the individual kinematic parameters of forward swimming and used the bout duration and the maximum TBF to represent bout intensity. When each bout was performed, we measured the maximum $\Delta f/f$ in a short window encompassing the bout. We used this maximum $\Delta f/f$ as a measure of the neuronal activity and correlated it with the kinematic parameters of each bout ([Figures 7F](#) and [7G](#)). For each cell in each larva, a linear regression was performed between the neuronal activity and the kinematic variable. [Figure 7F](#) shows the analysis for a representative larva, where neuronal activity was regressed against bout duration. Activity in MeLr and MeLc correlated significantly with bout duration, whereas that of MeLm and MeM did not ([Figure S6D](#)). Across all larvae, we found that 82% (31/38) of MeLr cells had activity which correlated significantly with bout duration ([Figure 7H](#)), suggesting a role of this cell type in the control of this behavioral variable. Neuronal activity was also regressed against maximum TBF (example larva shown in [Figure 7G](#), where both MeLr and MeLc show a significant correlation). We found that activity in 89% (16/18) of MeLc cells showed a significant correlation with maximum TBF ([Figure 7I](#)).

From these experiments involving imaging of neuronal activity, monitoring behavior, and correlation of the former to different features of the latter, we learned that the nMLF is active when larvae perform swim bouts. Furthermore, we concluded that activity in all four types of large nMLF cells was related to motor output, but differently so. The activity in MeLr and MeLc correlated well with bout duration and maximum TBF, respectively—kinematic parameters consistent with the ablation and stimulation experiments presented earlier ([Figures 4](#) and [5](#)). These findings reinforce the importance of anatomically mapping and functionally connecting the specific roles these large nMLF neurons play with their downstream targets in the spinal cord, a topic addressed in [Wang and McLean \(2014\)](#).

DISCUSSION

The OMR in larval zebrafish is comprised of orientation and locomotor movements in response to whole-field visual motion patterns and has been widely studied in the context of large-scale forward genetic screens for visuomotor defects ([Muto et al., 2005](#); [Neuhauss et al., 1999](#)) and psychophysical and physiological characterization of vision ([Maaswinkel and Li, 2003](#); [Orger et al., 2000](#)). Here we conducted a detailed quantitative descrip-

tion of locomotor behavior to dissect the variation and modulation of swimming in response to varying a single parameter of the visual stimulus: speed. This allowed us to better define the OMR as a visuomotor transformation from whole-field visual motion of different speeds to locomotor behavior. To better understand how the brain controls this visuomotor behavior, we investigated the nMLF, a multifunctional descending motor nucleus that is involved in a variety of behavioral contexts ([Gahtan et al., 2005](#); [Orger et al., 2008](#); [Sankrithi and O'Malley, 2010](#)). Stimulation and ablation of the nMLF suggested its participation in dynamically executing motor output required to achieve various speeds of swimming. When we performed functional calcium imaging in restrained, behaving larvae, we found that activity of the nMLF, and in particular two identifiable cells, MeLr and MeLc, is correlated with specific kinematic aspects of swimming: the bout duration and the maximum TBF.

For visual motion slower than 10 mm/s, larvae swim using mostly slow bouts. The kinematic parameters of these bouts are similar to the “slow-swim maneuver” ([Budick and O'Malley, 2000](#)), which constitutes a locomotor gait based on axial movement in conjunction with an alternating pectoral fin pattern ([Green et al., 2011](#)). We observe both these motifs in the electrical stimulation preparation when the fins are unrestrained (data not shown). Eliciting bouts more frequently and increasing their duration and intensity would permit modulation of this baseline motor pattern without changing the main components of the gait, consistent with our observations. When the speed of the visual motion exceeds 10 mm/s, larvae begin recruiting fast bouts. The responses to fast-moving gratings have values which resemble the kinematic features that describe “burst swimming,” a distinct gait primarily associated with the escape response ([Budick and O'Malley, 2000](#)). The OMR is generally considered to be a routine navigational behavior, and the ethological relevance in nature of visual motion at fast speeds in our assay that elicits these burst swims is unknown. Larvae can track whole-field visual motion well up to 20 mm/s, which suggests this is the upper limit of what they naturally encounter.

The complete circuit required to perform the OMR begins with the retina, which relays signals to the brain via ten identified retinal ganglion cell (RGC) arborization fields ([Figure 8](#)) ([Burrill and Easter, 1994](#); [Robles et al., 2011](#)). Identifying which arborization fields are involved in the OMR and how grating speed is encoded and transmitted to the locomotor circuitry elements such as the nMLF remains unknown. The OMR is known to persist in the absence of the optic tectum, the largest of these processing areas ([Roeser and Baier, 2003](#)), and when we imaged larvae expressing the fluorescent protein dendra under the control of a promoter that drives expression in RGCs (*atoh7/ath5*) ([Kay et al., 2001](#); [Masai et al., 2003](#)) we saw no regions of direct overlap with the RS population ([Figure S8](#)). This suggests connections are indirect and via nontectal retino-recipient areas such as the pretectum, recently identified to be involved in processing whole-field motion in zebrafish ([Kubo et al., 2014](#); [Portugues et al., 2014](#)). The nMLF has been implicated in other behaviors reliant on vision such as prey tracking and capture ([Bianco et al., 2011](#); [Borla et al., 2002](#); [Westphal and O'Malley, 2013](#)), since ablation of large cells impairs the ability of larvae to feed ([Gahtan et al., 2005](#)). Based on our findings, we suggest that

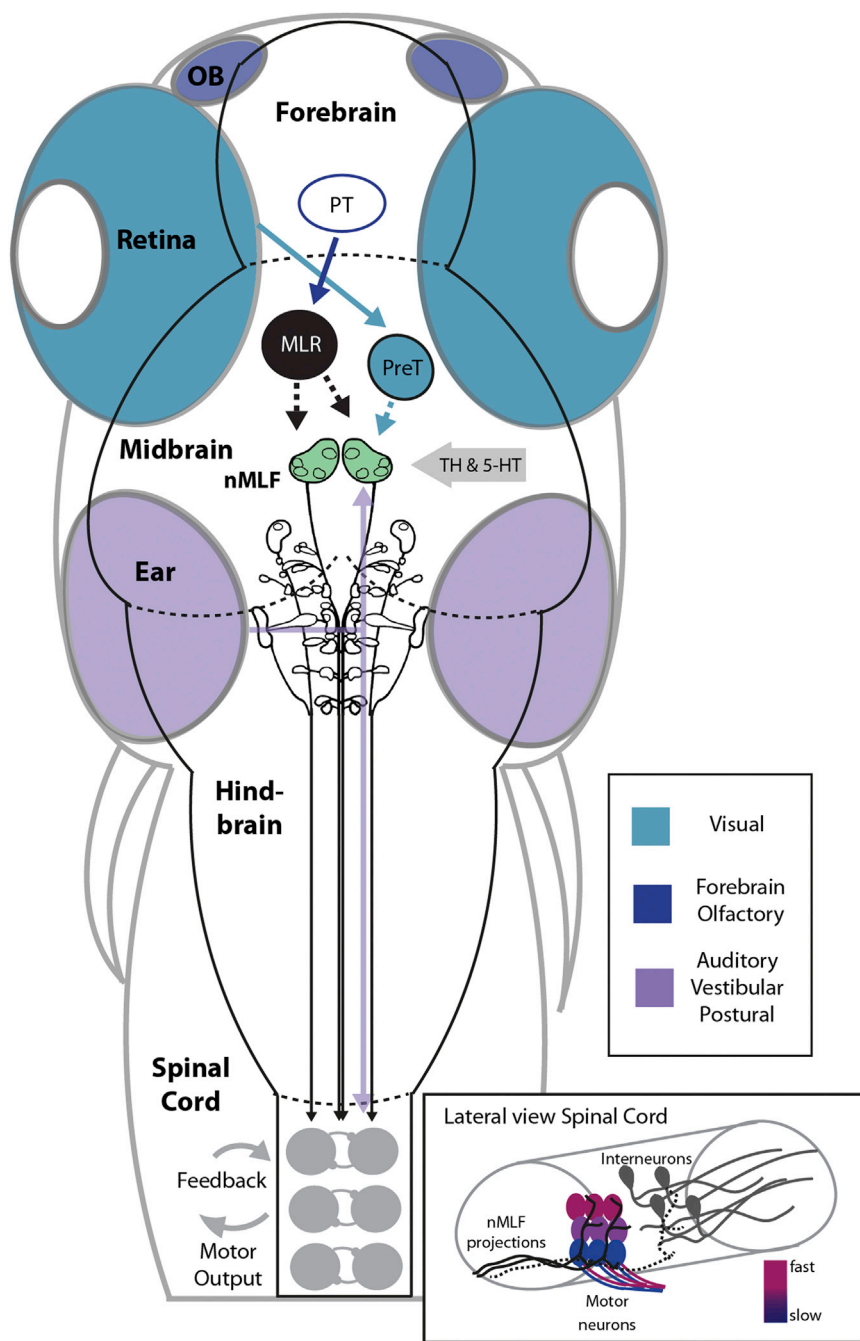


Figure 8. Schematic Model for the nMLF as a Center for Sensorimotor Processing and Locomotor Drive

Olfactory inputs are processed in the forebrain and have been functionally and anatomically linked to a pathway leading to the PT, the MLR, and to RS cells in closely related model systems. The MLR, if located in the larval zebrafish, would likely send bilateral cholinergic projections to the nMLF. Visual inputs from the retina are relayed to visual processing areas such as the pretectum, from where projections may be relayed to the nMLF (shown in green). There are significant TH and 5-HT projections surrounding the nMLF that could provide a source of neuromodulation. Vestibular inputs may be relayed via the tangential nucleus located next to the ear with projections to the nMLF. Together all of these inputs could be integrated in the nMLF to direct locomotion. The spinal cord is activated by descending glutamatergic inputs from the RS cells causing central pattern generators to oscillate, driving locomotor output and receiving proprioceptive feedback. Within the spinal cord (lateral view), there is a dorsal-ventral arrangement of activation with ventral spinal interneurons and motor neurons activated at slow swimming frequencies, and more dorsal recruitment as locomotor intensity must increase. Neurons from the nMLF innervate along a dorsal-ventral gradient in the spinal cord (Wang and McLean, 2014) that could specify the tonic excitation provided to where it is required in the spinal cord to produce a variety of speeds of locomotion. Abbreviations: 5-HT, serotonin; MLR, mesencephalic locomotor region; OB, olfactory bulb; PreT, pretectum; PT, posterior tuberculum; TH, tyrosine hydroxylase. Schematic of RS cells from Orger et al. (2008).

in the zebrafish, with no unidentified midbrain clusters of cholinergic cells observed in larval immunostaining (Arenzana et al., 2005). There are other neuromodulators thought to be present in the area immediately surrounding the nMLF, with identified terminals positive for TH and 5-HT (McLean and Fetcho, 2004), and dopaminergic and noradrenergic tracts targeting the area (Tay et al., 2011), but direct connections with nMLF neurons are not established. The tangential nucleus contributes to vestibular correction of eye position by relaying information sensed by utricular otoliths in the ear to oculomotor nuclei, with axonal arbors targeting the contralateral nMLF (Bianco et al., 2012) (Figure 8). This could provide a direct pathway for vestibular information to reach locomotor control centers. With these various sensory modalities providing inputs, the RS array could serve as an integration center for sensory cues directing navigation of the environment.

larvae lacking proper nMLF function may be unable to regulate bout duration and TBF well, reducing their capability to hunt.

It is interesting to consider inputs to the nMLF and RS cells important for sensorimotor integration. Olfactory inputs to motor control centers have been established in the lamprey from the olfactory epithelium to the RS cells, passing through the posterior tuberculum and the MLR (Figure 8) (Derjean et al., 2010). This connection from the cholinergic MLR is thought to drive bilateral RS cells symmetrically and monosynaptically from the MLR on one side (Brocard et al., 2010). The MLR has yet to be identified

The two bout types observed here in freely swimming larvae lead to an important question: how are the activity patterns

required to produce these different types of bouts produced by spinal CPGs? Work in the mammalian spinal cord revealed some of the complexity of glutamatergic inputs, showing that non-NMDA and NMDA receptor systems can function in parallel and independently to contribute to locomotor speed and stability (Talpalari and Kiehn, 2010). A new principle in spinal circuit organization has emerged in which different outputs arise from a shared pool of available neurons, through the selective recruitment of sets of multifunctional and specialized interneuron classes (Berkowitz et al., 2010). Many morphological classes of these interneurons and their genetic identities have been identified across vertebrate model organisms (Goulding, 2009; Hale et al., 2001; Roberts et al., 2010), and functional studies have revealed distinct patterns of activity across these identified interneuron types and their role in the generation of rhythmic locomotor patterns (Crone et al., 2009; Gosgnach et al., 2006; Wyart et al., 2009). In zebrafish, some excitatory classes of spinal interneurons are exclusively active during fast or slow swimming (McLean et al., 2008; Ritter et al., 2001). The dorsal-ventral position of these excitatory interneurons is correlated with the minimal swimming frequency at which the neuron is active (McLean et al., 2007), suggesting a utilization of a continuously varying set of interneuron cell types through smoothly graded shifts in locomotor speed.

The implementation of bouts and interbouts is shown here to be an important way larvae modulate swimming speed, and the spinal mechanisms controlling the duration and intensity of bouts are not known. In *Xenopus*, dedicated descending GABAergic “stopping” neurons (Li et al., 2003) or buildup of adenosine (Dale, 2002) may contribute to bout termination. Serotonin has been shown to reduce the interbout period, resulting in increased motor output, in active and fictive swimming (Brustein et al., 2003). Work incorporating network rhythmicity and intrinsic properties of motor neurons showed how zebrafish can accomplish increases in swimming frequency using a specific pattern of motor neuron recruitment (Menelaou and McLean, 2012), and this pattern of segregation of motor neuron pool by swimming frequency continues to adult stages (Ampatzis et al., 2013). Here we present behavioral observations where this broad range of swimming speeds has been experimentally evoked in an intact, nonparalyzed preparation, and this experimental paradigm provides an additional tool to study these CPG mechanisms.

Studies of anatomical links between nMLF cells and the spinal cord have shown a decrease in the density of collaterals with increasing distance along the tail (Gahtan and O'Malley, 2003). This is consistent with the idea of nMLF neurons providing a tonic signal to activate rostral spinal segments which then propagate a wave of excitation caudally to generate forward motion, and the spinal circuits necessary for episode duration control were recently localized to rostral segments (Wiggin et al., 2012). Wang and McLean (2014) make a leap forward by mapping both anatomical and synaptic connections between identified nMLF neurons and motor neuron targets. They show broad outputs from the nMLF to the spinal motor pool can be transformed into specific patterns of recruitment based on the intrinsic biophysical properties of motor neurons (Figure 8). Our observation that faster bouts elicited during the presentation of whole-field

motion are associated with increased activity in the nMLF would result in greater motor neuron activity, creating the more intense body bends we observe during responses to quickly moving gratings. Like motor neurons, excitatory spinal interneurons are also recruited in a dorsoventral pattern depending on the intensity of locomotion (Bhatt et al., 2007; McLean et al., 2007, 2008). The model that arises from these studies is that neurons within the nMLF may differentially innervate the spinal networks on the basis of axonal projections, but specific cells may differ in their targets. Both MeLr and MeLc may project to motor neurons, but MeLr may also activate interneurons regulating bout duration, while MeLc may project to interneurons regulating TBF. Thus, the nMLF could dictate not only motor neuron recruitment but also the participation of different premotor elements to coordinate appropriate responses to visual inputs.

In this study we attribute to the nMLF a major role in the control of the speed of locomotion. We believe the identification of how specific individual cells affect the behavioral parameters modulated when larvae swim at different speeds is an important step toward understanding the relationship between supraspinal control elements and locomotor output.

EXPERIMENTAL PROCEDURES

Animal Care

Fish were reared on a 14/10 hr light/dark cycle at 28°C. Animal handling and experimental procedures were approved by the Harvard University Standing Committee on the Use of Animals in Research and Training (Cambridge, MA, USA), by the Champalimaud Foundation Ethics Committee, and by the Portuguese Direcção Geral de Veterinária and were done according to the European Directive 2010/63/EU.

Freely Swimming Behavioral Assay

Tubingen WT zebrafish larvae 6 dpf swam freely in a 150 mm × 10 mm rectangular acrylic arena with 8 mm depth containing E3 medium. Their behavior was recorded from above at 700 Hz using an IR-sensitive high-speed camera (MC1362, Mikrotron), and IR illumination was provided from below. A sine wave grating with a spatial period of 10 mm drifting at different speeds was projected 5 mm below the larva using a DLP projector (BenQ). Stimulus presentations began when the larva remained for 5 s in one of the extremes of the arena and ended when the larva reached the opposite end or after 30 s had elapsed. Acquisition, stimulus presentation, tracking, and tail segmentation were performed online by a custom-written program (Visual C#, Microsoft). The location of the larva was determined by similar methods to previous studies (Burgess and Granato, 2007). See Supplemental Information.

Head-Embedded Behavioral Assay

The assay was performed as in Portugues and Engert (2011) except that the tail was tracked with custom-written software (Labview) in real time at 700 Hz. Trials 10 s long were separated by 30 s intertrial intervals during which the grating was static. The grating speeds (3, 5, 8, 10, 15, 20, 25, 30, and 40 mm/s) were presented five times in random order.

Two-Photon Laser Ablations and Testing Behavior

Nacre $-/-$ larvae 4 dpf were injected with Texas red dextran (TRD) as described previously (O'Malley et al., 1996; Orger et al., 2008; Supplemental Information), and recovered at 24–48 hr. Pre- and post-ablation behavior was tested individually in a 150 mm × 10 mm arena and imaged at 205 Hz with an MC1362 Mikrotron camera with IR illumination. Larvae were shown a forward grating for 10 s (at 5, 10, 20, or 30 mm/s), a stationary grating for 10 s, followed by a backward-moving grating at 10 mm/s for 20 s to return the larva to the initial side of the arena. Five trials per speed were presented in random order. Following this, larvae were embedded in 1.2% agarose and

imaged under a two-photon microscope. Reference stacks were acquired and then 4–8 cells were ablated and performed as previously described (Huang et al., 2013; Orger et al., 2008). Damage was well localized to the target region (Figure S3). Following ablation, larvae were unembedded and placed in a well with E3 medium to recover for at least 1 hr before postablation behavior was recorded, after which larvae were re-embedded and imaged 4–6 hr postablation where cell ablation was confirmed in 177/178 attempts.

Electrical Stimulation

A solution containing 10% calcium green dextran (CGD) and 10% TRD (both 3,000 MW, Invitrogen) in water was pressure injected using the same method. Larvae were embedded in 2% agarose and their tails freed. Glass pipettes of 33 m Ω resistance containing external solution and silver wire were connected to an SD-9 Grass stimulator. Stimulus pulses were 10 ms in duration. Five frequencies of stimulation (2, 4, 6, 8, and 10 pulses per second) between 0.30 and 0.60 μ A were selected in random order. Calcium responses from nMLF cells to electrical stimuli were recorded (Hamamatsu ORCA-ER CCD) at 20 Hz and analyzed using custom software (Labview and Matlab).

Two-Photon Imaging of nMLF Cells in Paralyzed Larvae

Larval zebrafish were spinally injected with CGD at 4 dpf as above and tested at 6–7 dpf. Larvae were paralyzed by immersion in 20 μ l of α -bungarotoxin solution (1 mg/ml in E3 medium) then embedded in 2% agarose and covered with E3 medium. The visual stimulus had ten trials of moving gratings, each lasting 10 s, with 10 s of static gratings in between trials. Data were analyzed using software custom written in Matlab. See [Supplemental Information](#).

Two-Photon Imaging in Behaving Larvae

The same injection and embedding protocol as above (without paralysis) was used, but the tail was freed. A total of 80 planes, 1 μ m apart encompassing all the nMLF were imaged for 120 s each. A visual stimulus consisting of a square-wave grating period of 1 cm was presented 5 mm below the larva, alternating every 10 s between static and moving in a caudal-to-rostral direction (speeds were 5, 10, and 30 mm/s, twice each per plane). Tail motion was tracked online at 200 Hz using a PikeF-032B camera (AVT) and IR illumination, allowing simultaneous monitoring of behavior and neural activity. Image time series were x-y motion corrected using Matlab software (David Heeger, New York University) and analyzed with custom-written Matlab software.

SUPPLEMENTAL INFORMATION

Supplemental Information includes eight figures, three movies, and Supplemental Experimental Procedures and can be found with this article online at <http://dx.doi.org/10.1016/j.neuron.2014.06.032>.

ACKNOWLEDGMENTS

The authors thank Filippo Del Bene for providing Ath5:Gal4;UAS:Dendra larvae (Arrenberg et al., 2009). K.E.S. received financial support from the Institut du Cerveau et de la Moelle épinière (ICM), the Philippe Foundation, and the European Research Council (ERC) starter grant OptoLoco. R.P. thanks the Human Frontier Science Program for funding through fellowship LT01115/2007-C. M.B.O. was supported by Marie Curie Career Integration Grant PCIG09-GA-2011-294049 and by the Fundação para a Ciência e a Tecnologia (FCT), PTDC/NEU-NMC/1276/2012. J.C.M. was supported by a PhD fellowship from the Portuguese Fundação para a Ciência e a Tecnologia. F.E. was supported by NIH grants DP1 NS082121 and R01DA030304. The authors thank Isaac Bianco, Adam Kampff, Kuo-Hua Huang, Tod Thiele, and Claire Wyatt for useful discussions and thank David McLean for critical reading of the manuscript and valuable comments.

Accepted: June 26, 2014

Published: July 24, 2014

REFERENCES

- Ahrens, M.B., Li, J.M., Orger, M.B., Robson, D.N., Schier, A.F., Engert, F., and Portugues, R. (2012). Brain-wide neuronal dynamics during motor adaptation in zebrafish. *Nature* 485, 471–477.
- Ampatzis, K., Song, J., Ausborn, J., and El Manira, A. (2013). Pattern of innervation and recruitment of different classes of motoneurons in adult zebrafish. *J. Neurosci.* 33, 10875–10886.
- Arenzana, F.J., Clemente, D., Sánchez-González, R., Porteros, A., Aijón, J., and Arévalo, R. (2005). Development of the cholinergic system in the brain and retina of the zebrafish. *Brain Res. Bull.* 66, 421–425.
- Arrenberg, A.B., Del Bene, F., and Baier, H. (2009). Optical control of zebrafish behavior with halorhodopsin. *Proc. Natl. Acad. Sci. USA* 106, 17968–17973.
- Berkowitz, A., Roberts, A., and Soffe, S.R. (2010). Roles for multifunctional and specialized spinal interneurons during motor pattern generation in tadpoles, zebrafish larvae, and turtles. *Front. Behav. Neurosci.* 4, 36.
- Bhatt, D.H., McLean, D.L., Hale, M.E., and Fetcho, J.R. (2007). Grading movement strength by changes in firing intensity versus recruitment of spinal interneurons. *Neuron* 53, 91–102.
- Bianco, I.H., Kampff, A.R., and Engert, F. (2011). Prey capture behavior evoked by simple visual stimuli in larval zebrafish. *Front. Syst. Neurosci.* 5, 101.
- Bianco, I.H., Ma, L.H., Schoppik, D., Robson, D.N., Orger, M.B., Beck, J.C., Li, J.M., Schier, A.F., Engert, F., and Baker, R. (2012). The tangential nucleus controls a gravito-inertial vestibulo-ocular reflex. *Curr. Biol.* 22, 1285–1295.
- Bilotta, J. (2000). Effects of abnormal lighting on the development of zebrafish visual behavior. *Behav. Brain Res.* 116, 81–87.
- Borla, M.A., Palecek, B., Budick, S., and O'Malley, D.M. (2002). Prey capture by larval zebrafish: evidence for fine axial motor control. *Brain Behav. Evol.* 60, 207–229.
- Brocard, F., Ryczko, D., Fenelon, K., Hatem, R., Gonzales, D., Auclair, F., and Dubuc, R. (2010). The transformation of a unilateral locomotor command into a symmetrical bilateral activation in the brainstem. *J. Neurosci.* 30, 523–533.
- Brustein, E., Chong, M., Holmqvist, B., and Drapeau, P. (2003). Serotonin patterns locomotor network activity in the developing zebrafish by modulating quiescent periods. *J. Neurobiol.* 57, 303–322.
- Buchanan, J.T., and Grillner, S. (1987). Newly identified 'glutamate interneurons' and their role in locomotion in the lamprey spinal cord. *Science* 236, 312–314.
- Budick, S.A., and O'Malley, D.M. (2000). Locomotor repertoire of the larval zebrafish: swimming, turning and prey capture. *J. Exp. Biol.* 203, 2565–2579.
- Burgess, H.A., and Granato, M. (2007). Modulation of locomotor activity in larval zebrafish during light adaptation. *J. Exp. Biol.* 210, 2526–2539.
- Burrill, J.D., and Easter, S.S., Jr. (1994). Development of the retinofugal projections in the embryonic and larval zebrafish (*Brachydanio rerio*). *J. Comp. Neurol.* 346, 583–600.
- Cabelguen, J.M., Bourcier-Lucas, C., and Dubuc, R. (2003). Bimodal locomotion elicited by electrical stimulation of the midbrain in the salamander *Notophthalmus viridescens*. *J. Neurosci.* 23, 2434–2439.
- Crone, S.A., Zhong, G., Harris-Warrick, R., and Sharma, K. (2009). In mice lacking V2a interneurons, gait depends on speed of locomotion. *J. Neurosci.* 29, 7098–7109.
- Dale, N. (2002). Resetting intrinsic purinergic modulation of neural activity: an associative mechanism? *J. Neurosci.* 22, 10461–10469.
- Delagina, T.G., Zelenin, P.V., and Orlovsky, G.N. (2002). Encoding and decoding of reticulospinal commands. *Brain Res. Brain Res. Rev.* 40, 166–177.
- Derjean, D., Moussaddy, A., Atallah, E., St-Pierre, M., Auclair, F., Chang, S., Ren, X., Zielinski, B., and Dubuc, R. (2010). A novel neural substrate for the transformation of olfactory inputs into motor output. *PLoS Biol.* 8, e1000567.

- Gahtan, E., and O'Malley, D.M. (2003). Visually guided injection of identified reticulospinal neurons in zebrafish: a survey of spinal arborization patterns. *J. Comp. Neurol.* *459*, 186–200.
- Gahtan, E., Tanger, P., and Baier, H. (2005). Visual prey capture in larval zebrafish is controlled by identified reticulospinal neurons downstream of the tectum. *J. Neurosci.* *25*, 9294–9303.
- Gosgnach, S., Lanuza, G.M., Butt, S.J., Saueressig, H., Zhang, Y., Velasquez, T., Riethmacher, D., Callaway, E.M., Kiehn, O., and Goulding, M. (2006). V1 spinal neurons regulate the speed of vertebrate locomotor outputs. *Nature* *440*, 215–219.
- Goulding, M. (2009). Circuits controlling vertebrate locomotion: moving in a new direction. *Nat. Rev. Neurosci.* *10*, 507–518.
- Green, M.H., Ho, R.K., and Hale, M.E. (2011). Movement and function of the pectoral fins of the larval zebrafish (*Danio rerio*) during slow swimming. *J. Exp. Biol.* *214*, 3111–3123.
- Grillner, S., Robertson, B., and Stephenson-Jones, M. (2013). The evolutionary origin of the vertebrate basal ganglia and its role in action selection. *J. Physiol.* *591*, 5425–5431.
- Haehnel, M., Taguchi, M., and Liao, J.C. (2012). Heterogeneity and dynamics of lateral line afferent innervation during development in zebrafish (*Danio rerio*). *J. Comp. Neurol.* *520*, 1376–1386.
- Häggglund, M., Borgius, L., Dougherty, K.J., and Kiehn, O. (2010). Activation of groups of excitatory neurons in the mammalian spinal cord or hindbrain evokes locomotion. *Nat. Neurosci.* *13*, 246–252.
- Hale, M.E., Ritter, D.A., and Fetcho, J.R. (2001). A confocal study of spinal interneurons in living larval zebrafish. *J. Comp. Neurol.* *437*, 1–16.
- Huang, K.H., Ahrens, M.B., Dunn, T.W., and Engert, F. (2013). Spinal projection neurons control turning behaviors in zebrafish. *Curr. Biol.* *23*, 1566–1573.
- Jordan, L.M. (1998). Initiation of locomotion in mammals. *Ann. N. Y. Acad. Sci.* *860*, 83–93.
- Kashin, S.M., Feldman, A.G., and Orlovsky, G.N. (1974). Locomotion of fish evoked by electrical stimulation of the brain. *Brain Res.* *82*, 41–47.
- Kay, J.N., Finger-Baier, K.C., Roeser, T., Staub, W., and Baier, H. (2001). Retinal ganglion cell genesis requires *lakritz*, a zebrafish atonal homolog. *Neuron* *30*, 725–736.
- Kimmel, C.B., Powell, S.L., and Metcalfe, W.K. (1982). Brain neurons which project to the spinal cord in young larvae of the zebrafish. *J. Comp. Neurol.* *205*, 112–127.
- Kimura, Y., Satou, C., Fujioka, S., Shoji, W., Umeda, K., Ishizuka, T., Yawo, H., and Higashijima, S.I. (2013). Hindbrain V2a neurons in the excitation of spinal locomotor circuits during zebrafish swimming. *Curr. Biol.* *23*, 843–849.
- Kohashi, T., and Oda, Y. (2008). Initiation of Mauthner- or non-Mauthner-mediated fast escape evoked by different modes of sensory input. *J. Neurosci.* *28*, 10641–10653.
- Koyama, M., Kinkhabwala, A., Satou, C., Higashijima, S., and Fetcho, J.R. (2011). Mapping a sensory-motor network onto a structural and functional ground plan in the hindbrain. *Proc. Natl. Acad. Sci. USA* *108*, 1170–1175.
- Kubo, F., Hablitzel, B., Dal Maschio, M., Driever, W., Baier, H., and Arrenberg, A.B. (2014). Functional architecture of an optic flow-responsive area that drives horizontal eye movements in zebrafish. *Neuron* *81*, 1344–1359.
- Li, W.C., Perrins, R., Walford, A., and Roberts, A. (2003). The neuronal targets for GABAergic reticulospinal inhibition that stops swimming in hatchling frog tadpoles. *J. Comp. Physiol. A Neuroethol. Sens. Neural Behav. Physiol.* *189*, 29–37.
- Maaswinkel, H., and Li, L. (2003). Spatio-temporal frequency characteristics of the optomotor response in zebrafish. *Vision Res.* *43*, 21–30.
- Masai, I.L., Lele, Z., Yamaguchi, M., Komori, A., Nakata, A., Nishiwaki, Y., Wada, H., Tanaka, H., Nojima, Y., Hammerschmidt, M., et al. (2003). N-cadherin mediates retinal lamination, maintenance of forebrain compartments and patterning of retinal neurites. *Development* *130*, 2479–2494.
- McDermid, J.R., and Drapeau, P. (2006). Rhythmic motor activity evoked by NMDA in the spinal zebrafish larva. *J. Neurophysiol.* *95*, 401–417.
- McLean, D.L., and Fetcho, J.R. (2004). Relationship of tyrosine hydroxylase and serotonin immunoreactivity to sensorimotor circuitry in larval zebrafish. *J. Comp. Neurol.* *480*, 57–71.
- McLean, D.L., Fan, J., Higashijima, S., Hale, M.E., and Fetcho, J.R. (2007). A topographic map of recruitment in spinal cord. *Nature* *446*, 71–75.
- McLean, D.L., Masino, M.A., Koh, I.Y., Lindquist, W.B., and Fetcho, J.R. (2008). Continuous shifts in the active set of spinal interneurons during changes in locomotor speed. *Nat. Neurosci.* *11*, 1419–1429.
- Menelaou, E., and McLean, D.L. (2012). A gradient in endogenous rhythmicity and oscillatory drive matches recruitment order in an axial motor pool. *J. Neurosci.* *32*, 10925–10939.
- Muto, A., Orger, M.B., Wehman, A.M., Smear, M.C., Kay, J.N., Page-McCaw, P.S., Gahtan, E., Xiao, T., Nevin, L.M., Gosse, N.J., et al. (2005). Forward genetic analysis of visual behavior in zebrafish. *PLoS Genet.* *1*, e66.
- Neuhauss, S.C.F., Biehlmaier, O., Seeliger, M.W., Das, T., Kohler, K., Harris, W.A., and Baier, H. (1999). Genetic disorders of vision revealed by a behavioral screen of 400 essential loci in zebrafish. *J. Neurosci.* *19*, 8603–8615.
- O'Malley, D.M., Kao, Y.H., and Fetcho, J.R. (1996). Imaging the functional organization of zebrafish hindbrain segments during escape behaviors. *Neuron* *17*, 1145–1155.
- Orger, M.B., Smear, M.C., Anstis, S.M., and Baier, H. (2000). Perception of Fourier and non-Fourier motion by larval zebrafish. *Nat. Neurosci.* *3*, 1128–1133.
- Orger, M.B., Kampff, A.R., Severi, K.E., Bollmann, J.H., and Engert, F. (2008). Control of visually guided behavior by distinct populations of spinal projection neurons. *Nat. Neurosci.* *11*, 327–333.
- Portugues, R., and Engert, F. (2009). The neural basis of visual behaviors in the larval zebrafish. *Curr. Opin. Neurobiol.* *19*, 644–647.
- Portugues, R., and Engert, F. (2011). Adaptive locomotor behavior in larval zebrafish. *Front. Syst. Neurosci.* *5*, 72.
- Portugues, R., Feierstein, C.E., Engert, F., and Orger, M.B. (2014). Whole-brain activity maps reveal stereotyped, distributed networks for visuomotor behavior. *Neuron* *81*, 1328–1343.
- Ritter, D.A., Bhatt, D.H., and Fetcho, J.R. (2001). *Vivo* imaging of zebrafish reveals differences in the spinal networks for escape and swimming movements. *J. Neurosci.* *21*, 8956–8965.
- Roberts, A., Li, W.C., Soffe, S.R., and Wolf, E. (2008). Origin of excitatory drive to a spinal locomotor network. *Brain Res. Brain Res. Rev.* *57*, 22–28.
- Roberts, A., Li, W.C., and Soffe, S.R. (2010). How neurons generate behavior in a hatchling amphibian tadpole: an outline. *Front. Behav. Neurosci.* *4*, 16.
- Robles, E., Smith, S.J., and Baier, H. (2011). Characterization of genetically targeted neuron types in the zebrafish optic tectum. *Front. Neural Circuits* *5*, 1.
- Roeser, T., and Baier, H. (2003). Visuomotor behaviors in larval zebrafish after GFP-guided laser ablation of the optic tectum. *J. Neurosci.* *23*, 3726–3734.
- Sankrithi, N.S., and O'Malley, D.M. (2010). Activation of a multisensory, multi-functional nucleus in the zebrafish midbrain during diverse locomotor behaviors. *Neuroscience* *166*, 970–993.
- Sato, T., Hamaoka, T., Aizawa, H., Hosoya, T., and Okamoto, H. (2007). Genetic single-cell mosaic analysis implicates ephrinB2 reverse signaling in projections from the posterior tectum to the hindbrain in zebrafish. *J. Neurosci.* *27*, 5271–5279.
- Shik, M.L., Severin, F.V., and Orlovski, G.N. (1966). Control of walking by means of electrical stimulation of the midbrain. *Biofizika* *11*, 659–666.
- Steeves, J.D., Sholomenko, G.N., and Webster, D.M.S. (1987). Stimulation of the pontomedullary reticular formation initiates locomotion in decerebrate birds. *Brain Res.* *401*, 205–212.

- Talpalar, A.E., and Kiehn, O. (2010). Glutamatergic mechanisms for speed control and network operation in the rodent locomotor CpG. *Front. Neural Circuits* 4, 19.
- Tay, T.L., Ronneberger, O., Ryu, S., Nitschke, R., and Driever, W. (2011). Comprehensive catecholaminergic projectome analysis reveals single-neuron integration of zebrafish ascending and descending dopaminergic systems. *Nat. Commun.* 2, 171.
- Wang, W.-C., and McLean, D.L. (2014). Selective responses to tonic descending commands by temporal summation in a spinal motor pool. *Neuron* 83. Published online July 24, 2014. <http://dx.doi.org/10.1016/j.neuron.2014.06.021>.
- Westphal, R.E., and O'Malley, D.M. (2013). Fusion of locomotor maneuvers, and improving sensory capabilities, give rise to the flexible homing strikes of juvenile zebrafish. *Front. Neural Circuits* 7, 108.
- Wiggin, T.D., Anderson, T.M., Eian, J., Peck, J.H., and Masino, M.A. (2012). Episodic swimming in the larval zebrafish is generated by a spatially distributed spinal network with modular functional organization. *J. Neurophysiol.* 108, 925–934.
- Wyart, C., Del Bene, F., Warp, E., Scott, E.K., Trauner, D., Baier, H., and Isacoff, E.Y. (2009). Optogenetic dissection of a behavioural module in the vertebrate spinal cord. *Nature* 461, 407–410.